QUADRATIC SPLINE APPROXIMATION OF THE CONTACT POTENTIAL FOR REAL-TIME SIMULATION OF LUMPED COLLISIONS IN MUSICAL INSTRUMENTS

Abhiram Bhanuprakash [*] *and Maarten van Walstijn*

Sonic Arts Research Centre (SARC)
Queen's University Belfast
Belfast, UK
{abhanuprakash01 | m.vanwalstijn}@qub.ac.uk

Vasileios Chatziioannou

Department of Music Acoustics (IWK)
University of Music and Performing Arts
Vienna, Austria
chatziioannou@mdw.ac.at

ABSTRACT

Collisions are an integral part of the sound production mechanism in a wide variety of musical instruments. In physics-based real-time simulation of such nonlinear phenomena, challenges centred around efficient and accurate root-finding arise. Nonlinearly implicit schemes are normally ill-suited for real-time simulation as they rely on iterative solvers for root-solving. Explicit schemes overcome this issue at the cost of a slightly larger error for a given sample rate. In this paper, for the case of lumped collisions, an alternate approach is proposed by approximating the contact potential curve. The approximation is described, and is shown to lead to a non-iterative update for an energy-stable nonlinearly implicit scheme. The method is first tested on single mass-barrier collision simulations, and then employed in conjunction with a modal string model to simulate hammer-string and slide-string interaction. Results are discussed in comparison with existing approaches, and real-time feasibility is demonstrated.

1. INTRODUCTION

Inter-object collisions are among the nonlinear acoustic phenomena that significantly influence the sonic character of various musical instruments. Certain collisions where contact occurs over a narrow region could be treated as *lumped*, e.g: piano hammer-string [1], xylophone mallet-bar [2] interaction, while others are generally regarded as *distributed*, e.g: sitar string-bridge [3], snare drum wire-membrane [4] interaction. These phenomena are often modelled by means of a Hertzian contact power law [5]. Partly owing to the one-sided nature of the nonlinearity, simulating them numerically in real-time - while preserving system properties critical in musical instrument simulation like passivity and stability - is a challenging task [6].

A range of energy-stable time-stepping schemes exists in the collision modelling literature. At one end of the spectrum we have *explicit* schemes [7, 8], where an auxiliary variable is introduced in order to quadratise the contact potential, which thereby allows the current system variable and the auxiliary variable to be explicitly expressed as functions of their previous values. Although this feature makes these schemes suited for real-time simulation, recent analysis [8] has revealed an inherent issue of the energy quadratisation approach: due to the dependency of the numerical energy on the auxiliary variable, these schemes do not exhibit a unique trajectory in the contact region of their phase-space, which can lead to increased errors. For example, perceptually significant wideband noise-like artefacts are produced in the case of a sitar-like configuration, suppressing which requires at least 4x oversampling [8].

At the other end of the spectrum lie *nonlinearly implicit* (NLI) schemes [6], where the current value of the system variable appears within a nonlinear implicit function. This leads to a transcendental equation to be solved at each time step, and for this purpose iterative solvers such as Newton's method have been traditionally employed. However, due to the uncertainty in the number of iterations, the computational cost of such schemes varies at each time step, and thus approaches employing iterative solvers are not well-suited for real-time simulation [7, 8].

Somewhere in between these two extremities lies another approach: to fix the power law exponent to unity and thereby obtain a specific non-iterative branched-form update for an NLI scheme [9]. This has since been adopted in a few case studies involving lumped collisions [10, 11]. However, such a model does not cover the full range of compliances involved in musical instruments - e.g., felt hammers in pianos have a large stiffness range for a given force range [12], and the measured power law exponent is generally around 2.5 [1]. In this paper, by approximating the contact potential curve, this approach is extended to the more general case of lumped collisions with any valid power law exponent.

2. LUMPED COLLISION MODEL

Throughout the paper, d_v and ∂_v denote the total and partial derivatives with respect to the variable v, respectively. Consider contact between two objects at positions u_1 and u_2 at time t, and let $y = y(t) := u_1(t) - u_2(t)$. If the contact occurs over a narrow region, the contact force F can be modelled in the form of a power law [5] as:

$$F(y) = -\kappa \big[y\big]_+^{\alpha} = -\partial_y V(y), \tag{1}$$

where the power law parameters $\kappa > 0$ and $\alpha \geq 1$ depend on the geometries and materials of the objects that come into contact. From Hertzian contact theory [5], the exponent α is typically 1 or 1.5. If one includes cases of strongly nonlinear compression of felts (e.g. kettledrum mallets [13] or piano hammer [14]), then $1 \leq \alpha \leq 3$ can be considered as a musically relevant range. With y now interpreted as a compression variable, $\big[y\big]_+ := \max(0, y)$ represents the inter-object compression, and

$$V(y) = \frac{\kappa}{\alpha+1}\big[y\big]_+^{\alpha+1} \tag{2}$$

[*] This work was supported by the European Union's Horizon 2020 research and innovation programme under the Marie Skłodowska-Curie grant agreement No 812719.

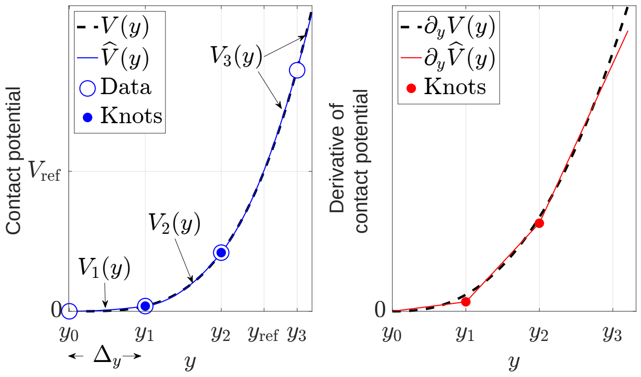

Figure 1: *Quadratic spline approximation of the contact potential (left, blue); its derivative (right, red), for* $\alpha = 2.5$ *and* $\Delta_y = 0.39\, y_{\rm ref}$ $(N = 3)$*. In both plots, the black dashed line shows the underlying power law.*

is the contact potential.

2.1. Quadratisation of the Contact Potential

Introducing an auxiliary variable ψ, the contact potential can be re-written [7] as

$$V = \frac{1}{2}\psi^2. \tag{3}$$

From (1) and (3), the contact force can then be written in terms of ψ and a new gradient variable $g := \partial_y \psi = \sqrt{\frac{1}{2}\kappa(\alpha+1)\,[y]_+^{\alpha-1}}$ as

$$F = -\psi\, g, \quad \mathrm{d}_t\psi = g\, \mathrm{d}_t y. \tag{4}$$

2.2. Quadratic Spline Approximation of the Contact Potential

In musical instrument modelling, one would typically have an estimate of the collision energy range which can be considered as a reference, say $[0, V_{\rm ref}]$. From (2), the corresponding reference compression range is $[0, y_{\rm ref}]$, where

$$y_{\rm ref} = \left[\frac{(\alpha+1)V_{\rm ref}}{\kappa}\right]^{\frac{1}{\alpha+1}}. \tag{5}$$

As shown in Figure 1, we can sample the contact potential curve at $(N+1)$ regularly spaced compression values $y_j = j\Delta_y,\ j = 0, 1, 2, ...N,\ \Delta_y > 0$, where N is such that the last compression value $y_N \in [y_{\rm ref}, y_{\rm ref} + \Delta_y]$, i.e, $N = \left\lceil \frac{y_{\rm ref}}{\Delta_y} \right\rceil$, where $\lceil . \rceil$ represents the ceiling operator. V can now be approximated in a piecewise-quadratic fashion as

$$\widehat{V}(y) = \begin{cases} V_j(y) & : y \in [y_{j-1}, y_j),\ j = 1, 2, ..., N-1, \\ V_N(y) & : y \geq y_{N-1}, \\ 0 & : \text{otherwise}, \end{cases} \tag{6}$$

where

$$V_j(y) = a_j y^2 + b_j y + c_j, \quad j = 1, 2, ..., N \tag{7}$$

is the $j^{\rm th}$ quadratic segment, with $V_j(y_j) = V(y_j)$ being the sampled data. For $\widehat{V}$ and its derivative $\partial_y \widehat{V}$ to represent a one-sided nonlinearity, we require both the first quadratic segment $V_1(y)$ and its derivative $\partial_y V_1(y)$ to pass through the origin. Further, for $\widehat{V}$ to be a continuous function, successive quadratic segments need to meet at their 'knots' $\{(y_j, V_j(y_j))\}, j = 1, 2, ..., N-1$, and for $\widehat{V}$ to be at least C^1 smooth, the first derivatives of successive segments need to be equal at their knots. These conditions can be written as

$$b_1 = c_1 = 0, \tag{8}$$

$$V_j(y_j) = V_{j+1}(y_j), \quad \text{and} \tag{9}$$

$$\partial_y V_j(y_j) = \partial_y V_{j+1}(y_j), \quad j = 1, 2, ...N-1. \tag{10}$$

The design parameter Δ_y controls the accuracy of the approximation - the accuracy is generally expected to increase as Δ_y is reduced (or equivalently, the number of quadratic segments N is increased). Now, with conditions (8) - (10) imposed, the piecewise-quadratic approximation $\widehat{V}$ in (6) becomes a quadratic spline approximation (QSA) of the contact potential. Here we compute the spline co-efficients $\{a_j, b_j, c_j, j = 1, 2, ..., N\}$ by adapting the recipe described for cubic splines in [15] for the case of quadratic splines, and solving a system of linear equations involving a bi-diagonal matrix (see companion website [1] for more detail).

One such $\widehat{V}$ and its derivative $\partial_y \widehat{V}$ (which is the corresponding linear spline approximation of $-F$) are shown in Figure 1. Notice that, with only 3 segments, the QSA seems to be quite close to the underlying contact potential curve, while the approximation is more visually apparent in the case of the first derivative.

Observations over a large range of κ, α and Δ_y suggest that $\widehat{V}$ is strictly convex. Eqs. (6) and (8) together with convexity imply that $\widehat{V}(y) \geq 0\,\forall\, y$. From the above, it is clear that $\widehat{V}$ has the same key features as V. Hence we can generally conclude that, for any system, approximating V by $\widehat{V}$ does not change the form of the energy balance, and energy-stable behaviour is preserved. Lastly, it is not difficult to see that $\widehat{V} = V$ for $\alpha = 1$, since in this case the underlying contact potential curve is quadratic for $y \geq 0$.

3. NUMERICAL PRELIMINARIES

Let $\Delta_t = 1/f_s$ denote the temporal step with sampling frequency f_s. Further, as per standard practice, let u^n be the numerical approximation of a variable u at time $t = n\Delta_t$. Let us now define elemental temporal difference and averaging operators:

$$\delta_t u^n := \frac{u^{n+\frac{1}{2}} - u^{n-\frac{1}{2}}}{\Delta_t}, \quad \mu_t u^n := \frac{u^{n+\frac{1}{2}} + u^{n-\frac{1}{2}}}{2}. \tag{11}$$

Derivatives of u can now be approximated by the following centred discrete operators:

$$\delta_{t\cdot} u^n := \delta_t \mu_t u^n = \frac{u^{n+1} - u^{n-1}}{2\Delta_t} \approx \partial_t u\Big|_{t=n\Delta_t}, \tag{12}$$

$$\delta_t^2 u^n := \delta_t\, \delta_t u^n = \frac{u^{n+1} - 2u^n + u^{n-1}}{\Delta_t^2} \approx \partial_t^2 u\Big|_{t=n\Delta_t}. \tag{13}$$

Similarly, the following centred discrete averaging operators can be defined:

$$\mu_{t\cdot} u^n := \frac{u^{n+1} + u^{n-1}}{2} \approx u\Big|_{t=n\Delta_t}, \tag{14}$$

$$\mu_t^2 u^n := \mu_t \mu_t u^n = \frac{u^{n+1} + 2u^n + u^{n-1}}{4} \approx u\Big|_{t=n\Delta_t}. \tag{15}$$

[1] Companion website: https://github.com/abhirambhanuprakash/qsa-LumpedCollisions

4. CASE STUDY I : MASS-BARRIER SINGLE COLLISIONS

A good starting point to investigate numerical schemes for the simulation of lumped collisions is the simple problem of a mass m colliding with a rigid barrier placed at u_{b}. Let $u = u(t)$ be the displacement of the mass at time t, and let u_0 and v_0 be the initial displacement and velocity of the mass, respectively. The equation of motion of the mass-barrier system can be written as

$$m\, \mathrm{d}_t^2 u = F(y) = -\partial_y V(y), \tag{16}$$

where the compression variable $y(t) := u(t) - u_{\mathrm{b}}$, and $F(y)$ and $V(y)$ are the contact force and potential as defined in (1) and (2), respectively.

4.1. Discretisation

Eq. (16) can be discretised as

$$m\, \delta_t^2 u^n = F^n. \tag{17}$$

Expanding (17) results in a nonlinear equation in s of the form

$$s + z - qF^n = 0, \tag{18}$$

where $s = y^{n+1} - y^{n-1}$ is the update step, $z = 2(u^{n-1} - u^n)$ is a history variable, and $q = \frac{\Delta_t^2}{m}$ is a constant. Based on how the contact force F is discretised, various numerical schemes are proposed in the literature. Here, bearing in mind that energy conservation and stability are critical in musical instrument simulation, we select two schemes having these key properties, described below.

4.1.1. Explicit scheme

Based on quadratising the contact potential as in (3), (4) can be discretised as

$$F^n = -(\mu_{t\cdot}\psi^n)g^n, \quad \delta_{t\cdot}\psi^n = g^n\, \delta_{t\cdot} y^n. \tag{19}$$

The second equation in (19) results in a separate update of ψ as

$$\psi^{n+\frac{1}{2}} = \psi^{n-\frac{1}{2}} + \frac{1}{2} g^n s, \tag{20}$$

which when substituted in (18) yields the solution

$$s = -\frac{z + q\psi^{n-\frac{1}{2}} g^n}{1 + \frac{1}{4} q (g^n)^2}. \tag{21}$$

A variant of this scheme bounds $\psi^{n+\frac{1}{2}} \geq 0$ and partly in order to respect this constraint, calculates g^n in a branched form (see section 3.3.6 in [8]). Here this variant (denoted EXP) is selected, as it has desirable properties such as a provably non-adhesive contact force [8].

4.1.2. Nonlinearly implicit scheme

Another choice of discretising F [6] is to use the discrete gradient:

$$F^n = -\frac{\delta_{t\cdot} V(y^n)}{\delta_{t\cdot} y^n} = -\frac{V(s + y^{n-1}) - V(y^{n-1})}{s}. \tag{22}$$

Substituting (22) in (18) gives the nonlinear equation

$$s + z + q\frac{V(s + y^{n-1}) - V(y^{n-1})}{s} = 0. \tag{23}$$

Because V is described by a power law, eq. (23) is a transcendental equation with the unknown s appearing implicitly within the nonlinear term. As mentioned in the introduction, traditionally the solution for s is obtained using iterative methods. Here, this NLI scheme updated by employing a Newton-Raphson solver is denoted IMP.

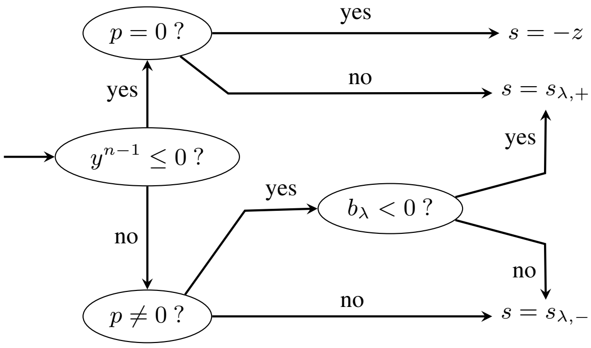

Figure 2: *Branched solution with the QSA method.*

With either scheme, once s is found, one can update the compression variable $y^{n+1} = s + y^{n-1}$ and then update the displacement as $u^{n+1} = y^{n+1} + u_{\mathrm{b}}$. The reader is referred to [8] for the energy balance equations of the system for both schemes.

4.2. A Non-Iterative Update for a Nonlinearly Implicit Scheme: The QSA Method

Starting from the same discretisation of F as the NLI scheme (eq. (22)) but with V replaced by $\widehat{V}$, we have the nonlinear equation

$$\underbrace{s + z + q\frac{\widehat{V}(s + y^{n-1}) - \widehat{V}(y^{n-1})}{s}}_{G(s)} = 0. \tag{24}$$

Following the argument in section 2.2 in [16], here using the convexity of $\widehat{V}$ we can show that $\mathrm{d}_s G(s) \geq 1$, and thereby $G(s)$ is not only monotonically increasing, but also has a unique root. Further exploiting the convexity of $\widehat{V}$, the solution to (24) can be expressed in branched-form, as illustrated by the flowchart in Figure 2, where

$$s_{\lambda,\pm} = \frac{-b_\lambda \pm \sqrt{b_\lambda^2 - 4a_\lambda c_\lambda}}{2a_\lambda}, \tag{25}$$

and where $\{a_\lambda, b_\lambda, c_\lambda\}$ are the coefficients of the quadratic $\lambda(s) := s\, G(s)$ (see companion website [1] for a derivation). Because the conditions of a particular branch might result in one or both of $\widehat{V}(s + y^{n-1})$ or $\widehat{V}(y^{n-1})$ collapsing to zero, $\lambda(s)$ takes different forms in different branches. The coefficients $\{a_\lambda, b_\lambda, c_\lambda\}$ for each branch are given in Table 1.

Table 1: *Coefficients of the quadratic $\lambda(s)$ for the branches in Figure 2.*

Branch	a_λ	b_λ	c_λ
$y^{n-1} \leq 0$, $p = 0$	1	z	0
$y^{n-1} \leq 0$, $p \neq 0$	$1{+}q\, a_p$	$z +$ $q\,(2a_p y^{n-1}{+}b_p)$	$q\, V_p(y^{n-1})$
$y^{n-1} > 0$, $p \neq 0$	$1{+}q\, a_p$	$z +$ $q\,(2a_p y^{n-1}{+}b_p)$	$q\,\{V_p(y^{n-1}){-}\widehat{V}(y^{n-1})\}$
$y^{n-1} > 0$, $p = 0$	1	z	$-q\,\widehat{V}(y^{n-1})$

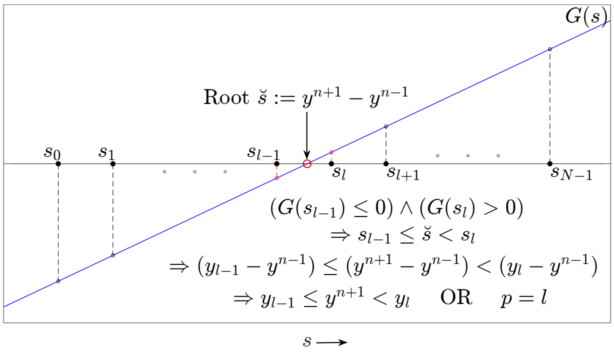
$G(s)$
Root $\breve{s} := y^{n+1} - y^{n-1}$
0
s_0
s_1
s_{l-1}
s_l
s_{l+1}
s_{N-1}
$(G(s_{l-1}) \leq 0) \wedge (G(s_l) > 0)$
$\Rightarrow s_{l-1} \leq \breve{s} < s_l$
$\Rightarrow (y_{l-1} - y^{n-1}) \leq (y^{n+1} - y^{n-1}) < (y_l - y^{n-1})$
$\Rightarrow y_{l-1} \leq y^{n+1} < y_l$ OR $p = l$
$s \longrightarrow$

Figure 3: *Logic to find the QSA segment index p.*

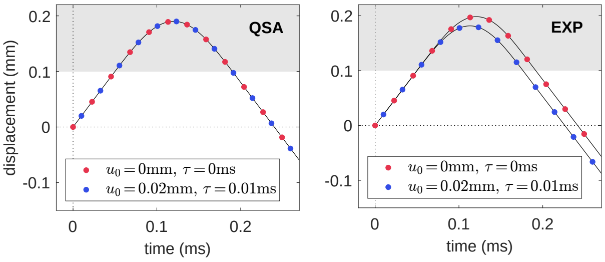

Figure 4: *Collisions of a mass with a stiff barrier for two initial displacements: with the QSA method with $N = 5$ (left), and with EXP (right). In both subplots, one of the simulations (blue) is time-shifted by τ such that the trajectories obtained by the two simulations overlap until the collision instant. In all simulations,* $\kappa = 10^8, \alpha = 1.3, m = 10\text{g}, v_0 = 2\text{ms}^{-1}$ *and* $\Delta_t = 1/44100$ s

4.2.1. Segment finding procedure

In the above, p represents the index of the quadratic spline segment that corresponds to the interval in which y^{n+1} lies. In other words,

$$p := \begin{cases} \left\lceil \frac{y^{n+1}}{\Delta_y} \right\rceil & : y^{n+1} > 0, \\ 0 & : \text{otherwise}. \end{cases} \tag{26}$$

Because $y^{n+1} = s + y^{n-1}$ is a shifted version of s, finding the y-interval in which y^{n+1} lies is equivalent to finding the s-interval in which the root $\breve{s}$ of $G(s)$ lies. Therefore, we take $y_j,\ j = 0, 1, 2, ..., N-1$ as test values for y^{n+1}, or equivalently, $s_j = y_j - y^{n-1}$ as test roots of $G(s)$, and evaluate $\{G(s_j)\}\ \forall j$. The index p is then determined as the one at which the sequence $\{G(s_j)\}$ changes sign from negative to positive. See Figure 3 for a pictorial sketch of this logic. If $G(s_0) > 0$, then it means that $\breve{s} < s_0$, which implies $y^{n+1} < y_0 = 0$, and hence $p = 0$. By a similar argument, for the other edge case where $G(s_{N-1}) < 0$, one can derive that $p = N$. This procedure involves at most N quadratic function evaluations at each time step, and therefore is not expected to be computationally intensive for a reasonably small N.

4.3. Numerical Simulation

Figure 4 depicts the displacement of a mass colliding with a stiff barrier as a function of time, simulated with the QSA method and EXP. For different initial displacements, the time-shifted trajectories obtained with the QSA method overlap, similar to IMP (not shown in figure). In contrast, in the case of EXP the trajectories diverge after the collision instant, showing an instance of larger error of the scheme due to a non-unique phase-space trajectory (see introduction).

5. CASE STUDY II : HAMMER-STRING INTERACTION

For a given number of segments, the QSA is expected to be less accurate for a larger α. Hence, piano hammer-string interaction, where $\alpha \approx 2.5$ [1] (see introduction), serves as a musically relevant edge case to investigate at most how many segments (N) are required for reasonably accurate simulations with the QSA method. To this end, we choose a stiff string model with simplified damping, omitting complex phenomena such as longitudinal modes, body coupling, etc., as in [8, 11]. The equations governing the motion of the hammer-string system [8] are given by

$$\rho A \partial_t^2 u = T\partial_x^2 u - EI\partial_x^4 u + 2\rho A(\eta_2 \partial_x^2 - \eta_0)\partial_t u + \mathcal{F}, \tag{27}$$

$$m_\text{h} \text{d}_t^2 w_\text{h} = -F, \tag{28}$$

where $u = u(x,t)$ is the displacement of the stiff string at time t and position x along its length L. ρ, A, T, E, I, η_2 and η_0 represent the string's mass density, area of cross section, tension, Young's modulus, moment of inertia, frequency-dependent and frequency-independent damping constants, while m_h and $w_\text{h} = w_\text{h}(t)$ denote the mass and displacement of the hammer, respectively. Given that the hammer comes into contact with the string over a narrow region around a point, the contact force density $\mathcal{F} = \mathcal{F}(x,t)$ can be modelled as

$$\mathcal{F} = \delta(x - x_\text{h})F, \tag{29}$$

where the dirac delta function $\delta(x - x_\text{h})$ represents the lumped interaction of the hammer at a fixed position x_h along the length of the string, and F is the hammer-string contact force as defined in eq. (1), with the hammer-string compression variable $y(t) := u(x_\text{h}, t) - w_\text{h}(t)$. Further, we assume simply-supported string boundary conditions

$$u(0,t) = 0, \quad u(L,t) = 0, \tag{30}$$

$$\partial_x^2 u(0,t) = 0, \quad \partial_x^2 u(L,t) = 0. \tag{31}$$

5.1. Modal Expansion

To ensure accurate string resonance frequencies, following [8], the solution to (27) is expanded as

$$u(x,t) = \sum_{i=1}^{M} v_i(x)\tilde{u}_i(t), \tag{32}$$

where $v_i(x) = \sin(\beta_i x)$ and $\beta_i = i\pi/L$ are the mode shape and wave number of the i^th mode, $\tilde{u}_i(t)$ is the i^th modal displacement, and M is the number of modes ($M \to \infty$ for an exact solution). Eq. (32) can be written concisely in vector-matrix form as

$$u = \mathbf{v}^T\,\tilde{\mathbf{u}}, \tag{33}$$

where $\mathbf{v} = \mathbf{v}(x)$ and $\tilde{\mathbf{u}} = \tilde{\mathbf{u}}(t)$ are Mx1 vectors whose i^th elements are $v_i(x)$ and $\tilde{u}_i(t)$, respectively. As done in [8, 10], substituting (32) in (27), pre-multiplying by $\mathbf{v}^T$ and spatially integrating over $[0, L]$ yields a set of modal ODEs

$$\tilde{m}\,\text{d}_t^2\tilde{\mathbf{u}} + \mathbf{R}\,\text{d}_t\tilde{\mathbf{u}} + \mathbf{K}\,\tilde{\mathbf{u}} = F\,\mathbf{h}, \tag{34}$$

where $\tilde{m} = \rho AL/2$ is the modal mass, and $\mathbf{R}$ and $\mathbf{K}$ are MxM positive definite diagonal matrices, and

$$\mathbf{h} = \mathbf{v}(x_\mathrm{h}) \tag{35}$$

is the Mx1 vector whose elements are the samples of the mode shapes at x_h. From (33) and (35), we can re-write y as

$$y = \mathbf{h}^T\tilde{\mathbf{u}} - w_\mathrm{h}. \tag{36}$$

5.2. Discretisation

Following [8], M is chosen such that the highest mode frequency is lesser than the Nyquist frequency $f_s/2$, and the modal string ODEs (34) are discretised as

$$\tilde{m}\ \delta_t^2\tilde{\mathbf{u}}^n + \widehat{\mathbf{R}}\ \delta_{t\cdot}\tilde{\mathbf{u}}^n + \widehat{\mathbf{K}}\ \mu_t^2\tilde{\mathbf{u}}^n = F^n\ \mathbf{h}, \tag{37}$$

where F^n is the discretised contact force as given by eq. (22) with

$$y^n = \mathbf{h}^T\tilde{\mathbf{u}}^n - w_\mathrm{h}^n \tag{38}$$

being the discrete version of the compression variable (36). $\widehat{\mathbf{R}}$ and $\widehat{\mathbf{K}}$ are MxM diagonal matrices with diagonal entries representing the damping and stiffness constants that are adjusted to compensate for numerical dispersion [8], respectively. Further, the hammer dynamics (28) are discretised as

$$m_\mathrm{h}\ \delta_t^2 w_\mathrm{h}^n = -F^n. \tag{39}$$

From eqs. (37) and (39), the update equations are derived as

$$\tilde{\mathbf{u}}^{n+1} = \tilde{\mathbf{u}}^{n-1} - \tilde{\mathbf{z}} + \mathbf{C}\ \mathbf{h}\ F^n, \tag{40}$$

$$w_\mathrm{h}^{n+1} = w_\mathrm{h}^{n-1} - z_\mathrm{h} - \xi_\mathrm{h}F^n, \tag{41}$$

where $\tilde{\mathbf{z}} = \mathbf{B}\tilde{\mathbf{u}}^{n-1} - \mathbf{A}\tilde{\mathbf{u}}^n$, $z_\mathrm{h} = 2(w_\mathrm{h}^{n-1} - w_\mathrm{h}^n)$, and $\xi_\mathrm{h} = \Delta_t^2/m_\mathrm{h}$. $\mathbf{A}$, $\mathbf{B}$ and $\mathbf{C}$ are MxM diagonal matrices with the i^{th} diagonal element depending on the natural frequency and decay rate of the i^{th} mode (see [8] for more detail). Pre-multiplying (40) by $\mathbf{h}^T$ and subtracting (41), we have the scalar update equation

$$\underbrace{y^{n+1} - y^{n-1}}_{s} + \underbrace{\left(\mathbf{h}^T\tilde{\mathbf{z}} - z_\mathrm{h}\right)}_{z} - \underbrace{\left(\mathbf{h}^T\mathbf{C}\mathbf{h} + \xi_\mathrm{h}\right)}_{q} F^n = 0, \tag{42}$$

which is of the same form as (18), and therefore we can solve for s non-iteratively by the branched-form solution of the QSA method (see Figure 2). Once we obtain s, we can update F^n from (42) as $F^n = (s+z)/q$, and then substitute the value of F^n in the string and hammer update equations (40) and (41) to update $\tilde{\mathbf{u}}^{n+1}$ and w_h^{n+1}, respectively.

For the continuous and discrete energy balance equations of the hammer-string system, the reader is referred to [8].

5.3. Numerical Simulation

Single hammer-string collisions were simulated with string and hammer parameters set to the measurements reported in [1]. As an inverse measure of the QSA method's 'accuracy' (with respect to the IMP result) we define a log normalised difference $\log_{10}\left(||\mathbf{F}_\mathrm{QSA} - \mathbf{F}_\mathrm{IMP}||/||\mathbf{F}_\mathrm{IMP}||\right)$, where $\mathbf{F}_\mathrm{QSA}$ and $\mathbf{F}_\mathrm{IMP}$ are the hammer forces as functions of time obtained by the QSA method and IMP, respectively. The hammer force evolutions in Figure 5 (left) suggest that generally the accuracy of the QSA method can be increased by reducing Δ_y, and the plot over a range of Δ_y in Figure 5 (right) confirms this trend.

Sounds of single hammer strikes were synthesised with low initial hammer velocity (1ms^{-1}) and high string damping ($\eta_0 = 8\mathrm{s}^{-1}$), with both the IMP and QSA methods, and with N varied from 2 to 30 in the QSA case (see companion website [1]). Listening to these sounds indicates that differences are barely noticeable for N larger than 13. In less extreme cases than the hammer-string interaction, a smaller N is expected to suffice for reasonably accurate simulation. The optimal value of N needs to be determined on a case-by-case basis.

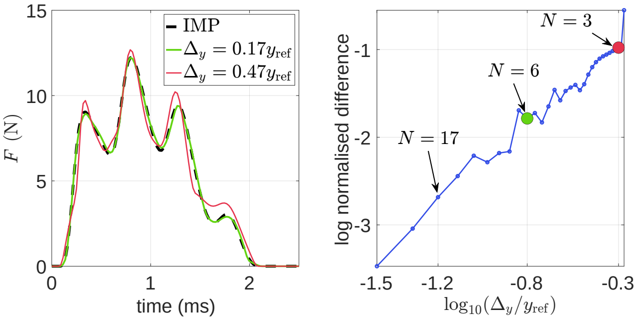

Figure 5: Left: *Hammer force evolutions for a single hammer strike for two Δ_y values (corresponding to $N = 3$ (red) and $N = 6$ (green)) compared with IMP (dashed black)*; Right: *Log of the normalised difference between the hammer force signals obtained with the QSA method and IMP as a function of* $\log_{10}(\Delta_y/y_\mathrm{ref})$. *Red and green circles correspond to the Δ_y values in the left plot. The initial hammer velocity is* 3.5ms^{-1}, $\kappa = 4.5$x$10^9, \alpha = 2.5$ *and* $\Delta_t = 1/44100$ s *for all cases.*

6. CASE STUDY III : SLIDE-STRING INTERACTION

Slide-string instrumentalists slide a cylindrical object (generally with their left hand) over a string to produce continuously-varying pitch patterns such as glissando and vibrato. In addition to this, they use the right-hand fingers to pluck/damp the string, and the left-hand finger trails the slide object to damp the non-speaking length of the string. The reason for choosing this case study is twofold: (a) from Hertzian contact theory, α is around 1.5 in this case [5], therefore the QSA method can be tested with α closer to unity, and (b) real-time performance can be tested with complex time-varying control inputs. To account for the time-varying slide contact and finger forces, we modify the model in (27) as [11]

$$\begin{aligned}\rho A\partial_t^2 u = T\partial_x^2 u - EI\partial_x^4 u + 2\rho A\left[\eta_2\partial_x^2 - \eta_0\right]\partial_t u \\ + \mathcal{F}_\mathrm{o} + \mathcal{F}_\mathrm{l} + \mathcal{F}_\mathrm{r},\end{aligned} \tag{43}$$

where the string parameters are as before, and $\mathcal{F}_\mathrm{o} = \mathcal{F}_\mathrm{o}(x,t)$, $\mathcal{F}_\mathrm{l} = \mathcal{F}_\mathrm{l}(x,t)$ and $\mathcal{F}_\mathrm{r} = \mathcal{F}_\mathrm{r}(x,t)$ are the slide contact, left-hand finger and right-hand finger force densities, respectively. Because the slide is cylindrical in shape, it comes into contact with the string over a narrow region and therefore, similar to the hammer-string case, $\mathcal{F}_\mathrm{o}$ can be modelled in a lumped fashion as

$$\mathcal{F}_\mathrm{o} = \delta(x - x_\mathrm{o})F, \tag{44}$$

where $x_\mathrm{o} = x_\mathrm{o}(t)$ is the slide contact position, and F is the slide-string contact force as defined in (1). As in [11], combining the excitation and damping action of the finger forces, $\mathcal{F}_\mathrm{l}$ and $\mathcal{F}_\mathrm{r}$ are phenomenologically modelled as

$$\mathcal{F}_\phi = \chi_\phi\left[F_{\phi,\mathrm{e}} + F_{\phi,\mathrm{R}}\right], \quad \phi = \mathrm{l},\mathrm{r} \tag{45}$$

where $F_{\phi,\mathrm{e}} = F_{\phi,\mathrm{e}}(t)$ and $F_{\phi,\mathrm{R}} = F_{\phi,\mathrm{R}}(t)$ are the excitation and damping forces, and $\chi_\phi = \chi_\phi(x,t)$ is the spatial distribution of finger ϕ, respectively. The finger damping force is modelled as being proportional to the magnitude of the finger excitation force, i.e.,

$$F_{\phi,\mathrm{R}}(t) = -r\,|F_{\phi,\mathrm{e}}(t)|\,\mathrm{d}_t u_\phi, \tag{46}$$

where r is a finger damping parameter, and

$$u_\phi = u_\phi(t) = \int_{x_\phi - W_\phi/2}^{x_\phi + W_\phi/2} \chi_\phi(x,t)\,u(x,t)\,dx \tag{47}$$

represents the spatially averaged string displacement at x_ϕ. Motivated by [10], here the spatial distributions are modelled as

$$\chi_\phi(x,t) = \begin{cases} \frac{\pi}{2W_\phi}\cos\left[\frac{\pi}{W_\phi}(x - x_\phi)\right] & : |x - x_\phi| \le \frac{W_\phi}{2}, \\ 0 & : \text{otherwise}, \end{cases} \tag{48}$$

where $x_\phi = x_\phi(t)$ and W_ϕ represent the centre and width of $\chi_\phi(x,t)$, respectively. In order to incorporate hand compliance in the model, the same string-slide-hand physical configuration as in [11] is chosen, featuring a slide-hand oscillator (SHO) formed by a slide mass m_o, a hand stiffness k_H and a hand damping parameter r_H, whose dynamics can be described by

$$m_\mathrm{o}\,\mathrm{d}_t^2 w_\mathrm{o} + r_\mathrm{H}\,\mathrm{d}_t(w_\mathrm{o} - w_\mathrm{H}) + k_\mathrm{H}\,(w_\mathrm{o} - w_\mathrm{H}) = -F, \tag{49}$$

where $w_\mathrm{o} = w_\mathrm{o}(t)$ and $w_\mathrm{H} = w_\mathrm{H}(t)$ are the displacements of the slide and hand, respectively. Note that $w_\mathrm{H}, x_\mathrm{o}, x_\phi$ and $F_{\phi,\mathrm{e}}$ are control inputs. Further, simply supported conditions (eqs. (30) and (31)) are assumed for this case study as well, as in [11].

6.1. Modal Expansion

Following the same recipe as in section 5.1, we substitute (32) in (43), pre-multiply by $\mathbf{v}^T$ and spatially integrate over $[0, L]$ to obtain the modal ODEs

$$\tilde{m}\,\mathrm{d}_t^2\tilde{\mathbf{u}} + \mathbf{R}\,\mathrm{d}_t\tilde{\mathbf{u}} + \mathbf{K}\tilde{\mathbf{u}} = F\,\mathbf{h}_\mathrm{o} + \sum_{\phi=\mathrm{l,r}} (F_{\phi,\mathrm{e}} + F_{\phi,\mathrm{R}})\,\mathbf{h}_\phi, \tag{50}$$

where $\tilde{m}$, $\mathbf{R}$ and $\mathbf{K}$ are as defined in section 5.1, and $\mathbf{h}_\mathrm{o}$ and $\mathbf{h}_\phi$ are time-varying Mx1 vectors, defined by

$$\mathbf{h}_\mathrm{o} = \mathbf{v}(x_\mathrm{o}(t)), \quad \text{and} \tag{51}$$

$$\mathbf{h}_\phi = \int_{x_\phi - W_\phi/2}^{x_\phi + W_\phi/2} \mathbf{v}(x)\,\chi_\phi(x,t)\,dx, \tag{52}$$

with $h_{\phi,i} = \frac{\pi^2\cos(\beta_i W_\phi/2)}{\pi^2 - \beta_i^2 W_\phi^2}\sin(\beta_i x_\phi(t))$ being the i^th element of $\mathbf{h}_\phi, i = 1, 2, ..., M$. Further, substituting (33) in (47), u_ϕ can be re-written as

$$u_\phi = \mathbf{h}_\phi^T\,\tilde{\mathbf{u}}. \tag{53}$$

As in the hammer-string case, from (33) and (51), we can write the slide-string compression variable $y := u(x_\mathrm{o}, t) - w_\mathrm{o}$ as

$$y = \mathbf{h}_\mathrm{o}^T\tilde{\mathbf{u}} - w_\mathrm{o}. \tag{54}$$

6.2. Energy Balance

Here, pre-multiplying (50) by $(\mathrm{d}_t\tilde{\mathbf{u}})^T$ and (49) by $\mathrm{d}_t w_\mathrm{o}$, the following energy balance equation for the modal slide-string formulation is derived:

$$\mathrm{d}_t H = (P_\mathrm{o} + \sum_{\phi=\mathrm{l,r}} P_\phi) - (Q_\mathrm{str} + Q_\mathrm{o} + \sum_{\phi=\mathrm{l,r}} Q_\phi), \tag{55}$$

where

$$\begin{aligned} H = \frac{1}{2}\tilde{m}||\mathrm{d}_t\tilde{\mathbf{u}}||^2 + \frac{1}{2}\tilde{\mathbf{u}}^T\mathbf{K}\tilde{\mathbf{u}} + \frac{1}{2}m_\mathrm{o}(\mathrm{d}_t w_\mathrm{o})^2 \\ + \frac{1}{2}k_\mathrm{H}(w_\mathrm{o} - w_\mathrm{H})^2 + V \end{aligned} \tag{56}$$

is the Hamiltonian, now with the extra potential energy term due to the hand stiffness k_H. P and Q are driving and dissipated powers, with subscripts o, str and ϕ representing the slide, the string and finger ϕ respectively, and are given by

$$\begin{aligned} P_\mathrm{o} = [r_\mathrm{H}\,\mathrm{d}_t w_\mathrm{o} - k_\mathrm{H}(w_\mathrm{o} - w_\mathrm{H})]\,\mathrm{d}_t w_\mathrm{H} \\ - F\,\partial_x u|_{x=x_\mathrm{o}}\mathrm{d}_t x_\mathrm{o}, \end{aligned} \tag{57}$$

$$P_\phi = (\mathrm{d}_t\tilde{\mathbf{u}})^T\mathbf{h}_\phi\left[F_{\phi,\mathrm{e}} - r|F_{\phi,\mathrm{e}}|(\mathrm{d}_t\mathbf{h}_\phi)^T\tilde{\mathbf{u}}\right], \tag{58}$$

$$Q_\mathrm{str} = (\mathrm{d}_t\tilde{\mathbf{u}})^T\mathbf{R}\,(\mathrm{d}_t\tilde{\mathbf{u}}), \quad Q_\mathrm{o} = r_\mathrm{H}\,(\mathrm{d}_t w_\mathrm{o})^2, \text{ and} \tag{59}$$

$$Q_\phi = r\,|F_{\phi,\mathrm{e}}|\,||(\mathrm{d}_t\tilde{\mathbf{u}})^T\mathbf{h}_\phi||^2. \tag{60}$$

Note that P_o involves terms proportional to the vertical and horizontal control input velocities $\mathrm{d}_t w_\mathrm{H}$ and $\mathrm{d}_t x_\mathrm{o}$, and P_ϕ contains a term due to the changing excitation position $(\mathrm{d}_t\mathbf{h}_\phi)$. Such terms are expected when there is time-variance [11, 17].

6.3. Discretisation

The modal ODEs in (50) are discretised as

$$\begin{aligned} \tilde{m}\delta_t^2\tilde{\mathbf{u}}^n + \widehat{\mathbf{R}}\,\delta_{t\cdot}\tilde{\mathbf{u}}^n + \widehat{\mathbf{K}}\,\mu_t^2\tilde{\mathbf{u}}^n = F^n\mu_{t\cdot}\mathbf{h}_\mathrm{o}^n \\ + \sum_{\phi=\mathrm{l,r}} (F_{\phi,\mathrm{e}}^n + F_{\phi,\mathrm{R}}^n)\,\mu_{t\cdot}\mathbf{h}_\phi^n, \end{aligned} \tag{61}$$

where $\widehat{\mathbf{R}}$ and $\widehat{\mathbf{K}}$ are the damping and stiffness diagonal matrices which compensate for numerical dispersion as before. The finger damping force (eq. (46)) is discretised as

$$F_{\phi,\mathrm{R}}^n = -r\,|F_{\phi,\mathrm{e}}^n|\,\delta_{t\cdot}u_\phi^n, \tag{62}$$

where from (53) we have

$$u_\phi^n = (\mathbf{h}_\phi^n)^T\,\tilde{\mathbf{u}}^n. \tag{63}$$

The SHO dynamics (eq. (49)) can be discretised as

$$m_\mathrm{o}\delta_t^2 w_\mathrm{o}^n + r_\mathrm{H}\,\delta_{t\cdot}(w_\mathrm{o}^n - w_\mathrm{H}^n) + k_\mathrm{H}\mu_t^2(w_\mathrm{o}^n - w_\mathrm{H}^n) = -F^n. \tag{64}$$

From (61) and (64), the following string and slide update equations can be derived:

$$\begin{aligned} \tilde{\mathbf{u}}^{n+1} &= \tilde{\mathbf{u}}^{n-1} - (\tilde{\mathbf{z}} - \tilde{\mathbf{e}}) \\ &\quad + \mathbf{C}\left\{F^n\mu_{t\cdot}\mathbf{h}_\mathrm{o}^n + \sum_{\phi=\mathrm{l,r}} (F_{\phi,\mathrm{e}}^n + F_{\phi,\mathrm{R}}^n)\,\mu_{t\cdot}\mathbf{h}_\phi^n\right\}, \end{aligned} \tag{65}$$

$$w_\mathrm{o}^{n+1} = w_\mathrm{o}^{n-1} - z_\mathrm{sho} - q_\mathrm{sho}\,F^n, \tag{66}$$

where

$$\tilde{\mathbf{z}} = \mathbf{B}\,\tilde{\mathbf{u}}^{n-1} - \mathbf{A}\,\tilde{\mathbf{u}}^n, \tag{67}$$

$$\tilde{\mathbf{e}} = \mathbf{C}\sum_{\phi=\mathrm{l,r}} F_{\phi,\mathrm{e}}^n\,\mu_{t\cdot}\mathbf{h}_\phi^n, \tag{68}$$

$$z_\mathrm{sho} = \frac{2\,(\mathcal{K}_\mathrm{H} + 1)\,w_\mathrm{o}^{n-1} + (\mathcal{K}_\mathrm{H} - 1)\,w_\mathrm{o}^n - \xi_\mathrm{o}\mathcal{T}_\mathrm{H}^n}{1 + \mathcal{K}_\mathrm{H} + \mathcal{R}_\mathrm{H}}, \text{ and} \tag{69}$$

$$q_\mathrm{sho} = \frac{\xi_\mathrm{o}}{1 + \mathcal{K}_\mathrm{H} + \mathcal{R}_\mathrm{H}}, \tag{70}$$

with **A**, **B** and **C** as defined in section 5.2. $\mathcal{K}_\mathrm{H} = \frac{k_\mathrm{H}\Delta_t^2}{4m_\mathrm{o}}$, $\mathcal{R}_\mathrm{H} = \frac{r_\mathrm{H}\Delta_t}{2m_\mathrm{o}}$, and $\xi_\mathrm{o} = \frac{\Delta_t^2}{m_\mathrm{o}}$ are constants, and

$$\mathcal{T}_\mathrm{H}^n = k_\mathrm{H}\,\mu_t^2 w_\mathrm{H}^n + r_\mathrm{H}\,\delta_{t\cdot} w_\mathrm{H}^n \qquad (71)$$

is a 'hand term' fully determined by the control input w_H^n and the hand compliance parameters k_H and r_H.

6.4. Solving for the Contact and Hand Damping Forces

To solve for the forces F^n and $F^n_{\phi,\mathrm{R}}$, a similar approach as in [10] is taken. Pre-multiplying (65) by $(\mathbf{h}_\mathrm{o}^n)^T$ and $(\mathbf{h}_\phi^n)^T$, $\phi = \mathrm{l},\mathrm{r}$, a set of three scalar equations is obtained as

$$s_\zeta = e_\zeta - z_\zeta + \theta_{\zeta\mathrm{o}}F^n + \sum_{\phi=\mathrm{l},\mathrm{r}} \theta_{\zeta\phi}F^n_{\phi,\mathrm{R}}, \quad \zeta = \mathrm{o},\mathrm{l},\mathrm{r} \qquad (72)$$

where $s_\zeta = \left(\mathbf{h}_\zeta^n\right)^T\left(\tilde{\mathbf{u}}^{n+1} - \tilde{\mathbf{u}}^{n-1}\right)$, $e_\zeta = \left(\mathbf{h}_\zeta^n\right)^T\tilde{\mathbf{e}}$, $z_\zeta = \left(\mathbf{h}_\zeta^n\right)^T\tilde{\mathbf{z}}$, $\theta_{\zeta\mathrm{o}} = \left(\mathbf{h}_\zeta^n\right)^T\mathbf{C}\,\mu_{t\cdot}\mathbf{h}_\mathrm{o}^n$ and $\theta_{\zeta\phi} = \left(\mathbf{h}_\zeta^n\right)^T\mathbf{C}\,\mu_{t\cdot}\mathbf{h}_\phi^n$. Now we use (62) to eliminate s_l and s_r. This allows expressing each of $F^n_{\mathrm{l},\mathrm{R}}$ and $F^n_{\mathrm{r},\mathrm{R}}$ as linear functions of F^n alone, which when substituted in the equation for s_o give us a single scalar string update equation

$$(\mathbf{h}_\mathrm{o}^n)^T\,\tilde{\mathbf{u}}^{n+1} = (\mathbf{h}_\mathrm{o}^n)^T\,\tilde{\mathbf{u}}^{n-1} - z_\mathrm{str} + q_\mathrm{str}F^n, \qquad (73)$$

where z_str is a combined 'history and excitation variable' and q_str is a linear combination of θ_oo, θ_ol and θ_or. Finally, subtracting (66) from (73) yields

$$\underbrace{y^{n+1} - y^{n-1}}_{s} + \underbrace{(z_\mathrm{str} - z_\mathrm{sho})}_{z} - \underbrace{(q_\mathrm{str} + q_\mathrm{sho})}_{q}F^n = 0, \qquad (74)$$

which is of the form in (18) and thus can be non-iteratively solved with the QSA method (see section 4.2). Once s is found, $F^n = (s+z)/q$ can be computed, and this can then be used to update $F^n_{\phi,\mathrm{R}}$, $\phi = \mathrm{l},\mathrm{r}$ from the linear relations obtained previously. The contact forces F^n and $F^n_{\phi,\mathrm{R}}$ are then substituted in (65) to update the modal displacements $\tilde{\mathbf{u}}^{n+1}$.

6.5. Numerical Energy Balance

Pre-multiplying (61) by $(\delta_{t\cdot}\tilde{\mathbf{u}}^n)^T$ and (64) by $\delta_{t\cdot}w_\mathrm{o}^n$, a numerical energy balance that is analogous to the continuous domain balance (eq. (55)) can be derived as

$$\delta_t H^n = (P_\mathrm{o}^n + \sum_{\phi=\mathrm{l},\mathrm{r}} P_\phi^n) - (Q_\mathrm{str}^n + Q_\mathrm{o}^n + \sum_{\phi=\mathrm{l},\mathrm{r}} Q_\phi^n), \qquad (75)$$

where the numerical Hamiltonian

$$\begin{aligned} H^{n+\frac{1}{2}} &= \frac{1}{2}\Big\{\tilde{m}||\delta_t\tilde{\mathbf{u}}^{n+\frac{1}{2}}||^2 + (\mu_t\tilde{\mathbf{u}}^{n+\frac{1}{2}})^T\widehat{\mathbf{K}}(\mu_t\tilde{\mathbf{u}}^{n+\frac{1}{2}}) \\ &+ m_\mathrm{o}(\delta_t w_\mathrm{o}^{n+\frac{1}{2}})^2 + k_\mathrm{H}(\mu_t^2(w_\mathrm{o}^{n+\frac{1}{2}} - w_\mathrm{H}^{n+\frac{1}{2}}))^2\Big\} \qquad (76) \\ &+ \mu_t V(y^{n+\frac{1}{2}}). \end{aligned}$$

The numerical driving and dissipation powers are

$$\begin{aligned} P_\mathrm{o}^n &= \left\{r_\mathrm{H}\delta_{t\cdot}w_\mathrm{o}^n - k_\mathrm{H}\mu_t^2(w_\mathrm{o}^n - w_\mathrm{H}^n)\right\}\delta_{t\cdot}w_\mathrm{H}^n \\ &\quad - F^n\left\{\frac{\delta_{t\cdot}(\mu_{t\cdot}u(x_\mathrm{o}^n, n\Delta_t))}{\delta_{t\cdot}x_\mathrm{o}^n}\right\}\delta_{t\cdot}x_\mathrm{o}^n, \qquad (77) \\ P_\phi^n &= \delta_{t\cdot}\tilde{\mathbf{u}}^n\mu_{t\cdot}\mathbf{h}_\phi^n\Big\{F^n_{\phi,\mathrm{e}} - r|F^n_{\phi,\mathrm{e}}|(\delta_{t\cdot}\mathbf{h}_\phi^n)^T\mu_{t\cdot}\tilde{\mathbf{u}}^n\Big\}, \qquad (78) \\ Q_\mathrm{str}^n &= (\delta_{t\cdot}\tilde{\mathbf{u}}^n)^T\widehat{\mathbf{R}}(\delta_{t\cdot}\tilde{\mathbf{u}}^n), \quad Q_\mathrm{o}^n = r_\mathrm{H}(\delta_{t\cdot}w_\mathrm{o}^n)^2, \text{ and} \qquad (79) \\ Q_\phi^n &= r|F^n_{\phi,\mathrm{e}}|\left\{(\delta_{t\cdot}\tilde{\mathbf{u}}^n)^T\mu_{t\cdot}\mathbf{h}_\phi^n\right\}^2. \qquad (80) \end{aligned}$$

6.6. Numerical Simulation

Slide gestures were simulated with the same control inputs and parameters as in Figure 3 in [11] and a three-slide musical phrase comprising slide attachment/detachment, glissando and vibrato was synthesised with both IMP and the QSA method (with $N = 5$). With both methods, the slide-string rattle could be heard, particularly just after the pluck releases in the sound examples [see companion website], and the time-variation of the harmonics is similar to the finite-difference (FD) model in [11] (which uses the branched-form solution restricted to unity α), with the excitation sustained via the energy injected by the time-variance of the control inputs.

For $\alpha = 1$ there is no audible difference between the sounds from the QSA method and IMP - this is expected because the QSA is exact in this case. With $\alpha = 1.5$, the collisions are slightly softer as expected with both methods. However, a subtle high frequency 'glitter'-like artefact can be heard in the background with the QSA method. This effect can be subdued by reducing N, which indicates that this is likely caused by jumps in the derivatives of the contact force introduced by segment switching.

A notable feature of the simulation with the model proposed here is the disappearance of the noise-like components that were mistaken for 'slide noise' in [11]. However, this has little to do with QSA, and can be attributed to the spatially exact mode shape sampling at the contact points in the modal formulation, which avoids the non-smooth (de)-interpolation used in [11]. For sound examples, the reader is referred to the companion website [1].

6.7. Computational Efficiency

Following [8, 17], real-time factor (RTF) is defined as the amount of time that passes with the computation of one second of audio output. With the assumption that the control parameters vary relatively slowly over time, in a Matlab simulation these were updated blockwise for every N_b samples, employing linear interpolation as in [17]. Average RTFs of a few updates that are part of the simulation loop are listed in Table 2. Note that the average RTF of the QSA solver is about 0.045, which shows that the proposed method does not contribute much to the runtime. The RTF of updates of the time-varying parameters (such as the mode shape vectors) reduces as N_b is increased, as some of the computationally expensive operations are performed only once per block. Including the time taken to memorise values, the RTF of the whole simulation is about 0.2 for $N_b = 64$.

7. CONCLUDING REMARKS

By means of approximating the contact potential curve with a quadratic spline, a non-iterative technique for the update of an NLI scheme

Table 2: *Average RTFs of QSA solver and updates within the simulation loop for various values of N_b*

N_b	**8**	**16**	**32**	**64**
QSA solver	0.050	0.047	0.041	0.040
Parameter updates	0.104	0.088	0.074	0.071
Linear string update	0.025	0.024	0.022	0.022

is proposed for the specific case of lumped collisions. The approximation retains key properties of the underlying Hertzian power law such as convexity and non-negativity, and thereby preserves salient features including: (a) the energy-stable behaviour of the continuous-domain system, and (b) the uniqueness of solution of the NLI scheme. Initial value problem simulations indicate that the uniqueness of the phase-space trajectories of the NLI scheme is also kept intact. Results on string-object interactions show that accuracy can be controlled by varying the number of spline segments N, and also suggest that a small N may be sufficient for musical instrument simulations. Further, a modal slide-string model is introduced, and continuous and numerical energy balances are derived. Simulations employing the proposed method demonstrate real-time feasibility under time-varying control inputs. Thus, without compromising on efficiency, the proposed method extends the branched-form solution to the case of non-unity α, side-stepping the issues associated with existing collision modelling techniques.

Nevertheless, as the adage goes - "there is no such thing as a free lunch", and the above benefits come with a few drawbacks. Firstly, the proposed method is not readily extendable to distributed collisions. This is because application of the method in a distributed scenario generally results in a system of coupled quadratic equations, and solving such a system is non-trivial. An exception to this is the specific case of a barrier with aligned grid [9], which is of little practical significance as this is often not the case in musical applications, for example, in guitar string/fretboard collisions, fret positions may not be aligned with the (regularly spaced) string grid. Further, due to the non-smooth nature of the contact force approximation, the latent higher-order derivative structure is broken and this likely causes the production of (mildly audible) high-frequency artefacts in sustained contact simulations. Although this issue is seemingly alleviated by deploying cubic and higher-order splines instead of quadratic splines, doing so would raise non-trivial questions around ensuring convexity of the approximation. Moreover, the authors' attempts at computing robust numerical solutions of higher-order polynomial equations indicate that it (a) is more computationally expensive than solving quadratic equations, and (b) is non-trivial, as finite precision could lead to large errors. The inquisitive reader is encouraged to refer to [18] in order to appreciate the intricacies of cubic equation solving.

8. REFERENCES

[1] A. Chaigne and A. Askenfelt, "Numerical simulations of piano strings. I. A physical model for a struck string using finite difference methods," *J. Acoust. Soc. Am.*, vol. 95, pp. 1112–1118, 1994.

[2] A. Chaigne and V. Doutaut, "Numerical simulations of xylophones. I. Time domain modeling of vibrating bars," *J. Acoust. Soc. Am.*, vol. 101, pp. 539–557, 1997.

[3] C. Vyasarayani, S. Birkett, and J. McPhee, "Modeling the dynamics of a vibrating string with a finite distributed unilateral constraint: Application to the sitar," *J. Acoust. Soc. Am.*, vol. 125, no. 6, pp. 3673–3682, 2009.

[4] S. Bilbao, "Time domain simulation and sound synthesis for the snare drum," *J. Acoust. Soc. Am.*, vol. 131, no. 1, pp. 914–925, 2012.

[5] V. L. Popov, *Contact Mechanics and Friction: Physical Principles and Applications*, Springer, Heidelberg, New York, 2010.

[6] S. Bilbao, A. Torin, and V. Chatziioannou, "Numerical modeling of collisions in musical instruments," *Acta Acustica united with Acustica*, vol. 101, no. 1, pp. 155–173, 2015.

[7] M. Ducceschi and S. Bilbao, "Non-iterative solvers for nonlinear problems: the case of collisions," in *Proc. 22nd Int. Conf. on Digital Audio Effects (DAFx-19)*, 2019, pp. 17–24.

[8] M. van Walstijn, V. Chatziioannou, and A. Bhanuprakash, "Implicit and explicit schemes for energy-stable simulation of string vibrations with collisions: Refinement, analysis, and comparison," *J. Sound and Vibration*, vol. 569, pp. 117 – 968, 2024.

[9] S. Bilbao, "Numerical modeling of string barrier collisions," in *Proc. Int. Symp. Musical Acoustics (ISMA 2014)*, 2014.

[10] M. van Walstijn, J. Bridges, and S. Mehes, "A real-time synthesis oriented tanpura model," in *Proc. Int. Conf. Digital Audio Effects (DAFx-16)*, 2016, pp. 175–182.

[11] A. Bhanuprakash, M. van Walstijn, and P. Stapleton, "A finite difference model for articulated slide-string simulation," in *Proc. Int. Conf. Digital Audio Effects (DAFx-20)*, 2020, pp. 195–202.

[12] D. Russell and T. Rossing, "Testing the nonlinearity of piano hammers using residual shock spectra," *Acustica*, vol. 84, no. 5, pp. 967–975, Sept. 1998.

[13] L. Rhaouti, A. Chaigne, and P. Joly, "Time-domain modeling and numerical simulation of a kettledrum," *J. Acoust. Soc. Am.*, vol. 105, no. 6, pp. 3545–3562, June 1999.

[14] A. Stulov, "Hysteretic model of the grand piano hammer felt," *J. Acoust. Soc. Am.*, vol. 97, no. 4, pp. 2577–2585, April 1995.

[15] R. H. Bartels, J. C. Beatty, and B. A. Barsky, *An introduction to splines for use in computer graphics & geometric modeling*, Morgan Kaufmann Publishers Inc., San Francisco, CA, USA, 1987.

[16] V. Chatziioannou and M. van Walstijn, "Energy conserving schemes for the simulation of musical instrument contact dynamics," *J. Sound and Vibration*, vol. 339, pp. 262–279, 2015.

[17] M. van Walstijn, V. Chatziioannou, and A. Bhanuprakash, "Tunable collisions: Hammer-string simulation with time-variant parameters," in *Proc. Int. Conf. Digital Audio Effects (DAFx-23)*, 2023.

[18] J. F. Blinn, "How to solve a cubic equation, part 5: Back to numerics," *IEEE Computer Graphics and Applications*, vol. 27, no. 3, pp. 78–89, 2007.